1-bit Graphene-based Reconfigurable Intelligent Surface Design in Ka-Band

S. I. Inácio, L. M. Pessoa
INESC TEC and Faculdade de Engenharia, Universidade do Porto, Porto, Portugal,
{sofia.i.inacio, luis.m.pessoa}@inesctec.pt

***Abstract*—This paper presents a 1-bit graphene-based reflective reconfigurable intelligent surface (RIS), namely a reflectarray antenna, that operates in the Ka-band (27 – 31 GHz). The reflectarray unit-cell features a simple structure with one metal layer, a Rogers RT5880 substrate and a Graphene Sandwich Structure (GSS) on top. The GSS comprises two layers of graphene separated by a diaphragm paper and a thin PVC layer to enhance its durability. The reflectarray can ensure a 1-bit phase shift resolution, by alternating the bias voltage applied to the graphene. The unit-cell simulation shows that the losses are around 3 dB over the studied band for both unit-cell states. An equivalent circuit model is presented to facilitate the analysis and design of GSS-based unit-cells. The full-wave simulation results of a 32×32 reflectarray indicate a gain of 25 dBi for a steering angle of 10 deg., displaying a 1 dB gain bandwidth of 15%, confirming the promise of the graphene-based radiating elements.**

***Index Terms*—reflectarray, reconfigurable intelligent surface, graphene, 1-bit phase resolution, beam scanning.**

I. Introduction

Graphene is a two-dimensional carbon material that has excellent electromagnetic, mechanical, electrical, and thermal properties [1]. One of the most compelling aspects of graphene is its ability to support the propagation of surface plasmon polaritons at THz and infrared frequencies. This gives it the ability to display a strong localization of the wave, moderate losses, and it's also tunable through chemical doping or electrical/magnetic bias [2]. However, for most applications that will have a significant impact on society and the economy in the coming years (such as wireless communications, imaging, and radar), the mmWave region (specifically 30-300 GHz) is the most advantageous due to graphene's good trade-off between device size and link range. In this frequency band, the electrical properties of graphene, e.g. its conductivity, change significantly. Unfortunately, graphene-only antennas cannot achieve good radiation efficiency, compared to copper-based ones, because of their lower conductivity [3]. However, a new approach has combined graphene's electrical tunability with the low loss of metals, to design antennas with both reconfigurable properties and high efficiency [4].

Reflectarray antennas have gained popularity in recent years due to their ability to combine the benefits of traditional reflector antennas and conventional phased array antennas. By controlling the element phases individually, reflectarray antennas can achieve a specific radiation beam. Additionally, the spatial feeding method eliminates energy loss and reduces design complexity. The array elements are typically located on a planar aperture, which can have various shapes such as circular, square, or other general shapes. The positioning of the feeding source can be centralized or offset, depending on the intended application.

This paper proposes a 1-bit reflective reconfigurable intelligent surface that utilizes graphene in a Graphene Sandwich Structure (GSS) for unit-cell phase change. In Section II, we delve into the unit-cell design, simulation, and analysis, equivalent circuit, highlighting the key properties of graphene that are essential to this work. Section III presents the reflectarray modelling, synthesis, and simulation results. Finally, Section IV provides the conclusions of this study.

II. 1-bit Graphene-based Unit-Cell

A. Graphene

Graphene's electromagnetic response is fundamentally determined by its dynamic surface conductivity. This conductivity is closely intertwined with the chemical potential or Fermi level of graphene [5]. When electromagnetic radiation is absorbed by the electrons in graphene, it causes intraband and interband transitions, which alter the material's conductivity. Intraband transitions dominate in the microwave/THz frequencies, while interband transitions are prevalent in the infrared/visible range [6]. The intraband conductivity follows the Drude model and can be determined by:

$$\sigma(\omega) = -\frac{jq^2 k_B T}{\pi\hbar^2(\omega - j2/\tau)}\left(\frac{\mu_c}{k_B T} + 2\ln\left(e^{-\frac{\mu_c}{k_B T}} + 1\right)\right), \quad (1)$$

where q is the charge of an electron, k_B is the Boltzmann constant, $\hbar$ is the reduced Planck constant, T is temperature, μ_c is the chemical potential and τ is the relaxation time. It is important to note that the validity of this expression depends on the condition: $\hbar\omega < 2|\mu_c|$, which is observed at THz and lower frequencies for moderate chemical potential values [5]. At these frequencies, the energy of electromagnetic waves is not enough to excite the interband transition of electrons bound by covalent bonds, so it does not affect the conductivity of graphene. However, at higher frequencies, interband contributions become significant and must be taken into consideration [2].

Fig. 1 illustrates the calculated sheet impedance of graphene ($Z_g = 1/\sigma$), using (1). It is worth noting that the chemical potential can dynamically modulate the sheet resistance of graphene in the microwave and mm-wave bands. In contrast,

the reactance of graphene tends to be very low at microwave frequencies. From this, it can be concluded that graphene exhibits frequency-independent behaviour at microwave frequencies, with a nearly resistive conductivity, that can be effectively controlled by the chemical potential [2], [5], [7].

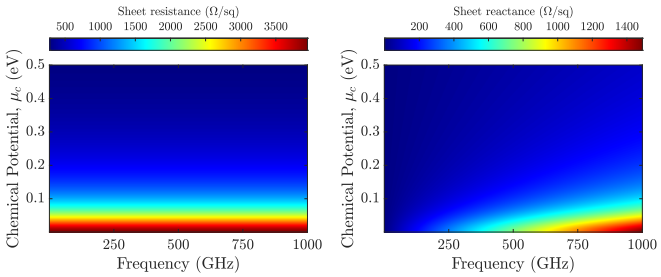

(a) (b)

Fig. 1. (a) Sheet resistance and (b) sheet reactance of graphene for several chemical potentials ($\tau = 0.06$ ps and $T = 300$ K).

B. Unit-Cell Design

In electromagnetic applications, obtaining a complete 2π phase coverage often requires modifying the sheet reactance of the material. Graphene is commonly used to design phase-related devices in THz or infrared frequencies for this reason, making it possible to achieve multi-bit devices [8], [7]. However, it can be challenging to control the wavefront of microwaves using graphene due to it's impedance characteristics, as seen in the previous section. For 1-bit graphene-based reflectarray antennas, or metasurfaces, the goal is to achieve consistent performance from two graphene-based elements. The reflection coefficients of the two elements should be almost identical in magnitude ($|\Gamma_1| = |\Gamma_2|$), but out of phase ($|\phi_1 - \phi_2| = \pi$).

Graphene's naturally thin, frequency-independent and tunable resistive properties also make it a promising material for amplitude-modulated microwave absorbers [9], [7], [5], [10]. In this regard, Balci et al. presented a Salisbury screen that replaces the conventional resistive film with a graphene-based sandwich structure (GSS) [9]. The device is based on the principle of controlling the phase shift caused by a resonance in the reflection coefficient, which appears when the GSS is placed at a quarter-wave distance from a metallic surface. The structure of the device allows for electrically adjustable resonance absorbance and a step-like phase shift around the resonance frequency when the graphene impedance matches the free space impedance.

Based on the previously presented concept, we designed a graphene-based unit-cell, with three main layers, for Ka-band (27–31 GHz). The square structure, with a side length of $p = 5$ mm, was optimized on CST, and shown in Fig. 2a. It comprises a 35 μm thick copper plane, a 1.575 mm Rogers RT5880 substrate ($\varepsilon_r = 2.2$, $\tan\delta = 0.0009$), and a GSS that consists of two square graphene patches (side length $p' = 4.85$ mm), with a 50 μm diaphragm paper layer soaked with ionic liquid (ε_r = 2.5) separating them. A 50 μm PVC top layer ($\varepsilon_r = 3.5$) is placed to enhance its durability and a FR4 layer (ϵ_r = 4.40, $\tan\delta = 0.02$) where the biasing lines are located.

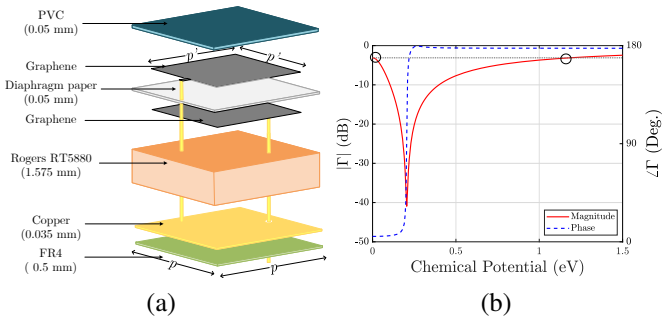

(a) (b)

Fig. 2. (a) Schematic view of the proposed graphene-based unit-cell and (b) magnitude and phase of the reflection coefficient as a function of the chemical potential at 29 GHz.

Fig. 2b displays the obtained reflection coefficient at 29 GHz for graphene's chemical potential values in the range of 0 to 1.5 eV. It is observed that the magnitude of the reflection coefficient shows a resonance at 0.2 eV, where half of the equivalent sheet resistance of graphene matches with the free space impedance. At the same chemical potential, a shift of π in the phase occurs. Although this is a universal behaviour, this configuration allows the electronic manipulation of the resonance condition, by tuning the charge density. In [9] this effect was achieved with bias voltages up to 2 V, at 12 GHz, with a similar structure.

To obtain a reflective binary unit-cell with almost identical reflection coefficient magnitudes, it is necessary to use a graphene chemical potential around 0 and 1.2 eV (as shown in Fig. 2b with a black doted line). Although this last value is relatively high, we believe it can be achieved with the presented unit-cell structure. According to [5], the GSS is a highly effective technique for enhancing doping efficiency, in contrast to the conventional method of direct gating of the graphene sheet.

Fig. 3 illustrates the magnitude and phase of the reflection coefficient for two distinct chemical potential values, namely 0 eV and 1.2 eV, from 27 GHz to 31 GHz. Within this range, we can observe that the magnitude remains almost constant and uniform between both states, while the phase difference fluctuates within the range of $180° \pm 20°$. This performance is in line with recent works on reconfigurable pin diode-based unit-cells [11], [12].

The results presented in Fig. 3b show that the reflection coefficient phase remains constant, at approximately 180º, across the entire range, for mu_c value of 1.2 eV. This happens because the reflection occurs in the GSS instead of in the copper layer, which is the case when the chemical potential is 0 eV. The small fluctuations in the phase difference can be attributed to the substrate thickness, which was not adjusted accurately for the whole frequency range.

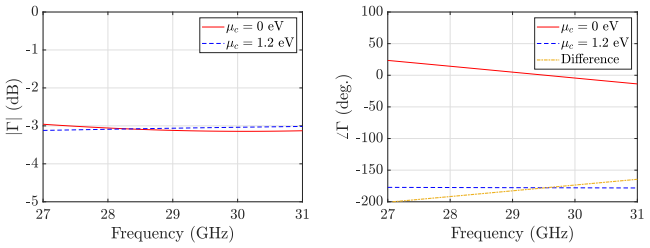

(a) (b)

Fig. 3. (a) Magnitude and (b) phase of the reflection coefficients.

C. Equivalent Circuit Model

In order to introduce the equivalent circuit model method for design and study of the proposed reflective graphene metasurface unit-cell, let's first assume that the graphene patch are now sized to match the cell. The proposed equivalent lumped circuit model is depicted in Fig. 4 [13], [9], [10]. Given that the thickness of graphene is significantly smaller than its skin depth in microwaves, one can represent the surface impedance of the graphene layers using their sheet resistance (R_g) and reactance (L_g) [9]. The calculation methodology for this representation is demonstrated in section II-A. The unit-cell layers, namely PVC, electrolyte and substrate, are represented by a transmission line with their thicknesses (t_p, t_e and t_s, respectively) and wave impedances (Z_p, Z_e and Z_s, respectively). Considering the low electron mobility in the electrolyte layer, it can be regarded as a dielectric.

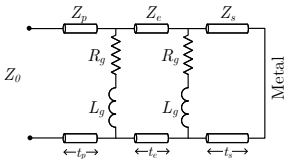

Fig. 4. Equivalent circuit model of the unit-cell without gap.

To maintain independence between the unit-cells, it is crucial to ensure that the graphene layers remain separate from each other. This is achieved by leaving a small gap, $g = p - p'$, between the graphene layers, as illustrated in Fig. 2a. In this work we assumed a square graphene patch. When a plane wave strikes the surface, the gaps between the graphene patches, of two neighbouring unit-cells, impact the circuit model, introducing a series capacitor to the layer impedance, as shown in Fig. 5. The total layer impedance is then obtained by summing up the two impedances [13]:

$$Z_g = AZ_{graphene} + Z_{gap} \ , \tag{2}$$

where A is an area filling ratio $\left(A = \frac{p^2}{p'^2}\right)$. The capacitive reactance of a graphene layer, in a GSS, is approximately:

$$Z_{gap} \approx -j\frac{Z_{\text{eff}}}{4\alpha} \ , \tag{3}$$

where

$$\alpha = \frac{pk_{\text{eff}}}{\pi} \ln\left[\frac{1}{\sin\left(\frac{\pi g}{2p}\right)}\right] . \tag{4}$$

Z_{eff} and k_{eff} are the wave impedance and wavenumber in the effective medium, respectively (ε_{eff} is the average relative permittivity of the mediums surrounding the graphene patches) [13], [14]. So, the capacity is achieved through:

$$C_{gap} \approx \frac{1}{\pi}\varepsilon_0\varepsilon_{\text{eff}} p \ln\left[\frac{1}{\sin\left(\frac{\pi g}{2p}\right)}\right] . \tag{5}$$

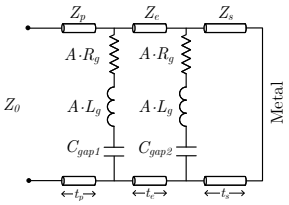

Fig. 5. Equivalent circuit model of the unit-cell with a gap.

The square shape of the patch, with both sides having equal gaps, results in the structure exhibiting equal impedances when exposed to TE and TM modes. However, if the graphene patch was made rectangular, a linearly polarized incident wave could be converted into a circularly polarized wave [13].

The simulation results for the configuration depicted in Fig. 5 are shown in Fig. 6, for chemical potentials of 0 and 1.2 eV. The results were obtained in CST, using unit-cell boundary conditions, and in Advance Design System (ADS), with the equivalent circuit model. The lumped element values are provided in Table I. Comparing the two analysis, the maximum phase error within the given frequency range was 0.4°, for both chemical potentials. Additionally the maximum magnitude error was observed to be 0.004 dB and 0.12 dB for the chemical potentials of 0 and 1.2 eV, respectively.

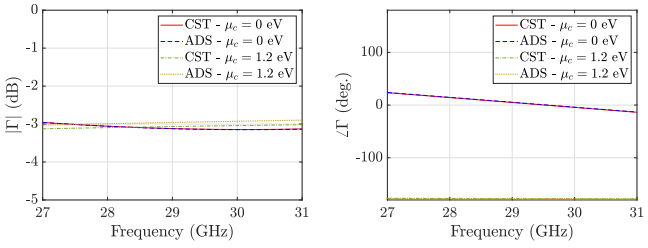

(a) (b)

Fig. 6. Reflection coefficient (a) magnitude and (b) phase obtained in CST and ADS for $\mu_c = 0$ eV and $\mu_c = 1.2$ eV.

From this analysis, it can be inferred that the graphene patch in a GSS unit-cell can be represented as a series network of R, L, and C components. The capacitance is solely dependent on the structural parameter, while the resistance and the inductance rely not only on the structural parameter but also on the Fermi energy of the graphene [15]. By applying a bias

TABLE I
EQUIVALENT CIRCUIT LUMPED ELEMENT VALUES

Chemical Potential	$\mu_c = 0$ eV	$\mu_c = 1.2$ eV
$A \cdot R_g$	4.20 kΩ	125 Ω
$A \cdot L_g$	252 pH	7.52 pH
C_{gap1}	0.129 pF	0.129 pF
C_{gap2}	0.101 pF	0.101 pF

voltage between the two graphene patches, the R_g and L_g can be actively controlled, due to the change in the chemical potential, μ_c, as described in (1).

It is important to note that the gap size, g, should be limited since a larger gap means a greater chemical potential value is required to achieve the same magnitude of reflection coefficient. This occurs because $A \cdot R_g$ increases as the gap increases, requiring a larger chemical potential value to obtain the same $A \cdot R_g$ value.

III. GRAPHENE-BASED RECONFIGURABLE REFLECTARRAY

After characterizing the reflection response of unit-cells, they were arranged to form an array. A graphene-based 1-bit reflectarray with 32×32 unit-cells was designed on CST Studio Suite, as shown in Fig. 7. To illuminate the reflectarray, a standard 13-dBi horn is used, positioned at a focal distance of 128 mm ($F/D = 0.8$). The horn is conveniently aligned to the centre of the reflectarray antenna for simplicity.

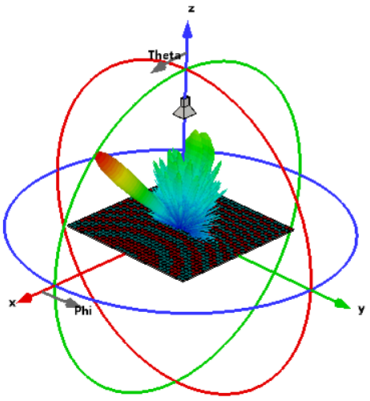

Fig. 7. The adopted scenario in the CST simulation of a reflectarray of 32×32 unit-cells and the 3D radiation pattern pattern in 45° direction.

Reflectarrays and classic planar antenna arrays share some similarities, but there is an additional consideration regarding reflectarrays. The position of the feed antenna is crucial in reflectarrays, as the electromagnetic fields released by the feed antenna propagate as a spherical wave from its phase centre [16]. The incident electromagnetic fields on the reflectarray aperture have a phase proportional to their travelled distance, called spatial phase delay. The phasing elements of the reflectarray need to compensate for this phase in order to create a collimated beam. A progressive phase can be added to the aperture to scan this beam in any direction, as in classic planar antenna arrays. So, the required phase shift of the mn^{th} element, to compensate for the spatial delay and to add a progressive phase to the aperture, to direct the beam to a certain spherical direction (θ_0, ϕ_0), is given by:

$$\phi_{mn} = k(R_{mn} - \sin\theta_0(x_m \cos\phi_0 + y_n \sin\phi_0)) + \varphi_0 \ , \quad (6)$$

where the Cartesian coordinates of each element are expressed as (x_m, y_n), R_{mn} is the distance from the feed phase centre to the mn element, k is the wavenumber at the centre frequency, and φ_0 is a phase constant [16]. However, ϕ_{mn} ranges from 0° to 360°, and since each element has only two states, 1-bit discrete phases are necessary. So, ϕ_{mn} in (6) is quantized in two levels, such as:

$$\phi^q_{mn} = \begin{cases} 180° & \text{(state “1”)}, \quad 90° < \phi_{mn} < 270° \\ 0° & \text{(state “0”)}, \quad \text{otherwise} \end{cases} . \quad (7)$$

Using discrete phases in reflectarrays can result in phase quantization errors if the number of levels is low. Unfortunately, these errors degrade the radiation performance of the reflectarray, leading to a decrease in aperture efficiency and in antenna gain [15], [17].

Fig. 8 depicts the phase distributions necessary for different steering angles [10°:10°:60°] and the corresponding 2D directivity patterns in the plane $\phi = 0°$ at 29 GHz, for steering angles [−60°:60°], obtained in CST. Due to the fact that the horn is covering the broadside angle of the reflection plane, the reflection in that direction is not taken into consideration. The 3D radiation pattern for a reflection towards 45° is shown in Fig. 7

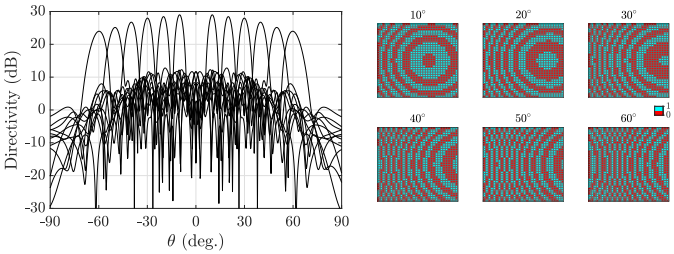

(a) (b)

Fig. 8. (a) The directivity patterns for different steering angles obtained in CST (b) The different phase distributions for the positive steering angles (for the negative, it is symmetric).

Table II presents the key performance parameters of the design graphene-based reflectarray, for a steering angle of $\theta = 10°$, obtained through simulation on CST.

Fig. 9 shows the gain as a function of frequency, obtained through simulation on CST, using the 10° distribution phase. The peak gain obtained was 24.9 dBi for the centre frequency. Due to beam squint the gain values at, exactly, 10° are slightly lower (red dashed line). For the peak gain (blue continuous line), the 1 dB gain bandwidth covers the whole frequency band, which corresponds to 15%. This value compares very favourably with the review of the performance of various works on Ka-band reflectarray antennas presented in [18].

TABLE II
REFLECTARRAY SPECIFICATIONS

Aperture size	160 mm × 160 mm
Number of elements	1024
Focal Distance	128 mm
Polarization	Linear
Element's spacing	$\sim \lambda/2$
Operating frequency range	$27 - 31$ GHz
Directivity	27.5 dBi
Gain	24.9 dBi
1-dB Gain BW	15 %
Scan angle	-60° to 60°

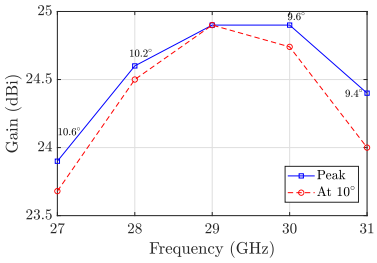

Fig. 9. Gain versus frequency for $\theta = 10°$.

IV. CONCLUSION

In this work we have presented an electronically reconfigurable graphene-based unit-cell design that achieves a 1-bit phase shift by changing the chemical potential of graphene in a GSS structure. An equivalent circuit model was proposed to analyse and design the unit-cell. It was concluded that an R-L-C series circuit could model the graphene layer even with a gap. The results obtained from CST and ADS demonstrate that this circuit can be used to study the unit-cell and optimize it, making it a promising tool for future research.

To demonstrate the effectiveness of the design, a 32×32 elements reflectarray was designed, illuminated by a standard horn. The full-wave simulation directivity patterns show that a reconfigurable reflectarray is feasible, displaying a 1 dB gain bandwidth of 15% (the whole studied band) confirming the promise of the graphene-based radiating elements.

Our future work will use the proposed unit-cell design to fabricate a reflectarray and obtain validation through experimental results. Producing graphene at a large scale and low cost can be challenging, so we aim to explore and establish cost-effective techniques for developing high-quality graphene-based components. Additionally, we intend to adapt this configuration to higher frequencies, around 100 GHz. Graphene-based reflectarrays show promising potential in overcoming the limitations posed by diodes and micro-electro-mechanical systems at those higher frequencies, where they become lossy and too large to be integrated within individual unit-cells. The incorporation of graphene simplifies the design and allows for a faster reconfiguration of the device.

ACKNOWLEDGMENT

This work was carried out in the framework of project SUPERIOT, which received funding from the Smart Networks and Services Joint Undertaking (SNS JU) under the European Union's Horizon Europe research and innovation programme under Grant Agreement No 101096021, including funding under the UK government's Horizon Europe funding guarantee, UKRI Grant Reference Number 10053751. This work was supported by FCT/MCTES (Portuguese Foundation for Science and Technology) under grant 2020.04948.BD.

REFERENCES

[1] M. J. Chashmi, P. Rezaei, and N. Kiani, "Polarization controlling of multi resonant graphene-based microstrip antenna," *Plasmonics*, vol. 15, no. 2, pp. 417–426, 2020.

[2] D. Correas-Serrano and J. S. Gomez-Diaz, "Graphene-based antennas for terahertz systems: A review," *arXiv preprint arXiv:1704.00371*, 2017.

[3] M. Dragoman, D. Neculoiu, A.-C. Bunea, G. Deligeorgis, M. Aldrigo, D. Vasilache, A. Dinescu, G. Konstantinidis, D. Mencarelli, L. Pierantoni *et al.*, "A tunable microwave slot antenna based on graphene," *Applied Physics Letters*, vol. 106, no. 15, p. 153101, 2015.

[4] J. Wang, W.-B. Lu, Z.-G. Liu, A.-Q. Zhang, and H. Chen, "Graphene-based microwave antennas with reconfigurable pattern," *IEEE Transactions on Antennas and Propagation*, vol. 68, no. 4, pp. 2504–2510, 2019.

[5] J. Zhang and W. Zhu, "Graphene-based microwave metasurfaces and radio-frequency devices," *Advanced Photonics Research*, vol. 2, no. 11, p. 2100142, 2021.

[6] B. Sensale-Rodriguez, R. Yan, M. M. Kelly, T. Fang, K. Tahy, W. S. Hwang, D. Jena, L. Liu, and H. G. Xing, "Broadband graphene terahertz modulators enabled by intraband transitions," *Nature communications*, vol. 3, no. 1, pp. 1–7, 2012.

[7] H. Chen, W.-B. Lu, Z.-G. Liu, and M.-Y. Geng, "Microwave programmable graphene metasurface," *Acs Photonics*, vol. 7, no. 6, pp. 1425–1435, 2020.

[8] K. Moradi, A. Pourziad, and S. Nikmehr, "A frequency reconfigurable microstrip antenna based on graphene in terahertz regime," *Optik*, vol. 228, p. 166201, 2021.

[9] O. Balci, N. Kakenov, and C. Kocabas, "Controlling phase of microwaves with active graphene surfaces," *Applied Physics Letters*, vol. 110, no. 16, 2017.

[10] X. Huang, X. Zhang, Z. Hu, M. Aqeeli, and A. Alburaikan, "Design of broadband and tunable terahertz absorbers based on graphene metasurface: equivalent circuit model approach," *IET Microwaves, Antennas & Propagation*, vol. 9, no. 4, pp. 307–312, 2015.

[11] J.-B. Gros, V. Popov, M. A. Odit, V. Lenets, and G. Lerosey, "A reconfigurable intelligent surface at mmwave based on a binary phase tunable metasurface," *IEEE Open Journal of the Communications Society*, vol. 2, pp. 1055–1064, 2021.

[12] S. Gharbieh, R. D'Errico, and A. Clemente, "Reconfigurable intelligent surface design using pin diodes via rotation technique–proof of concept," in *2023 17th European Conference on Antennas and Propagation (EuCAP)*. IEEE, 2023, pp. 1–4.

[13] I. Mazraeh-Fard and A. Alighanbari, "Equivalent circuit model for the analysis and design of graphene-based tunable terahertz polarizing metasurfaces," *Applied Optics*, vol. 61, no. 19, pp. 5760–5768, 2022.

[14] X. He, Y. Yao, Z. Zhu, M. Chen, L. Zhu, W. Yang, Y. Yang, F. Wu, and J. Jiang, "Active graphene metamaterial absorber for terahertz absorption bandwidth, intensity and frequency control," *Optical Materials Express*, vol. 8, no. 4, pp. 1031–1042, 2018.

[15] S.-G. Zhou, G. Zhao, H. Xu, C.-W. Luo, J.-Q. Sun, G.-T. Chen, and Y.-C. Jiao, "A wideband 1-bit reconfigurable reflectarray antenna at ku-band," *IEEE Antennas and Wireless Propagation Letters*, vol. 21, no. 3, pp. 566–570, 2021.

[16] P. Nayeri, F. Yang, and A. Z. Elsherbeni, "Reflectarray antennas: theory, designs, and applications," 2018.

[17] H. Yang, F. Yang, S. Xu, M. Li, X. Cao, J. Gao, and Y. Zheng, "A study of phase quantization effects for reconfigurable reflectarray antennas," *IEEE antennas and wireless propagation letters*, vol. 16, pp. 302–305, 2016.

[18] M. H. Dahri, M. H. Jamaluddin, F. C. Seman, M. I. Abbasi, A. Y. Ashyap, M. R. Kamarudin, and O. Hayat, "A novel asymmetric patch reflectarray antenna with ground ring slots for 5g communication systems," *Electronics*, vol. 9, no. 9, p. 1450, 2020.